5. CONCLUSION

A novel CPW-fed broadband antenna with wide square slots has been presented. By using the linear-taper technique, a 40% bandwidth of −10-dB return loss has been achieved. Changing the connection area has been shown to have little influence on the radiation patterns. The radiation patterns remained stable in the entire band and the cross-polarization level was very low. It can be predicted that this taper technique, which will be studied further, will be useful for other slot antennas.

ACKNOWLEDGMENT

This work was supported by the Natural Science Foundation of China (grant no. 60071020).

REFERENCES

1. C.Y. Huang and K.L. Wong, Coplanar waveguide-fed circularly polarized microstrip antenna, IEEE Trans Antennas Propagat 48 (2000), 328–329.
2. T. Girard, R. Staraj, and E. Cambiaggio, Comformal microstrip antenna arrays fed by bent coplanar waveguides, Electron Lett 34 (1998), 226–227.
3. S.S. Garcia and J.J. Laurin, Study of a CPW inductively coupled slot antenna, IEEE Trans Antennas Propagat 47 (1999), 58–64.
4. Y.D. Lin and S.N. Tsai, Coplanar waveguide-fed uniplanar bow-tie antenna, IEEE Trans Antennas Propagat 45 (1997), 305–306.
5. J.S. Chen and S.Y. Lin, Triple-frequency rectangular-ring slot antennas fed by CPW and microstrip line, Microwave Opt Technol Lett 37 (2003), 243–246.
6. T.F. Huang, S.W. Lu, and P. Hsu, Analysis and design of coplanar waveguide-fed slot antenna array, IEEE Trans Antennas Propagat 47 (1999), 1560–1565.
7. E.A. Soliman, S. Brebels, P. Delmotte, G.A.E. Vandenbosch, and E. Beyne, Bow-tie slot antenna fed by CPW, Electron Lett 35 (1999), 514–515.
8. M. Miao, B.L. Ooi, and P.S. Kooi, Broadband CPW-fed wide slot antenna, Microwave Opt Technol Lett 25 (2000), 206–211.

A METHOD FOR THE DETERMINATION OF A DISTRIBUTED FET NOISE MODEL BASED ON MATCHED-SOURCE NOISE-FIGURE MEASUREMENTS

M. C. Maya, A. Lázaro, and L. Pradell
Universitat Politècnica de Catalunya (UPC)
Dept. TSC, Campus Nord UPC
Mòdul D3, 08034, Barcelona, Spain

Received 24 October 2003

ABSTRACT: *A new method for the determination of a distributed FET noise model is presented. It is based on the extraction of the intrinsic noise-correlation matrix of an elemental section of the device from the device's noise figure, measured for only one source-impedance state at a number of frequency points. Experimental results up to 40 GHz are given.* © 2004 Wiley Periodicals, Inc. Microwave Opt Technol Lett 41: 221–225, 2004; Published online in Wiley InterScience (www.interscience.wiley.com). DOI 10.1002/mop.20099

Key words: *noise-parameters measurement; FET noise parameters; FET distributed noise model; intrinsic noise-correlation matrix; noise modeling*

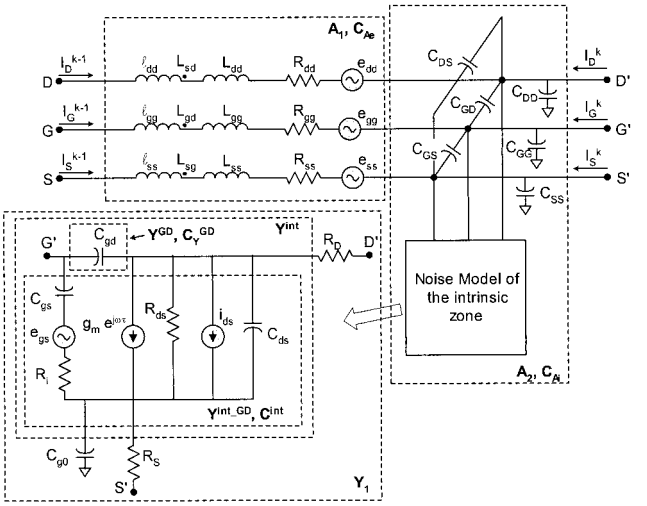

Figure 1 Schematic of an FET elemental section including the associated noise sources

1. INTRODUCTION

Distributed circuit models for FETs have been proposed in the literature for taking into account propagation effects along the device electrodes when the transistor dimensions, in particular its gate width, become of the same order of magnitude as the wavelength [1–3]. Distributed-noise analysis in MESFETs has also been developed [4] by including elemental noise sources in every elemental gate-width section of the FET small-signal model, and evaluating the total device noise-correlation matrix by adding the contributions from all sections. Regarding the elemental intrinsic-noise sources (see Fig. 1), a number of configurations have been considered; for example, the RPC noise model [5] is used in [4], while in [6] a simplified distributed noise model with no correlation between noise sources [7] is assumed. In order to include the FET distributed noise effects into foundry models and microwave CAD, the elemental intrinsic-noise sources are extracted, through a de-embedding procedure, from the four transistor-measured noise parameters (NPs), $F_{\min}$, Γ_{opt} (for both magnitude and phase), and R_n, provided that the device-distributed equivalent circuit is known [6]. In turn, the transistor NPs are determined by measuring their noise figure for a constellation of source impedances presented, at every frequency, to the transistor input by using a "tuner" (that is, a tuner-based method [8]).

In this paper, a new method to determine a distributed noise model for FETs is presented. It is based on measuring the transistor noise figure for an arbitrary source impedance (for convenience, a well-matched 50Ω source is used), unique at every frequency, to directly extract (using the knowledge of distributed small-signal circuit elements determined from the device-measured S parameters) the intrinsic distributed noise sources. The advantages of this method, compared to tuner-based methods [8], are setup simplicity (no tuner is required, only a conventional noise source), higher measurement speed, lower cost, avoiding FET oscillations (which may occur for some tuner reflection coefficients), and enhanced accuracy due to its smaller sensitivity to the device $|\Gamma_{\text{opt}}|$ [9]. In contrast with [6], a general intrinsic noise model, which includes two correlated noise sources in a hybrid configuration (see Fig. 2), is assumed. Moreover, to improve the model accuracy, it is assumed that the intrinsic noise-correlation matrix elements have a frequency dependence given by a smooth, low-order polynomial [9]. The distributed model is based in the so-called sliced model [6, 10, 11]. As a particular case, the uncorrelated "noise temperature"

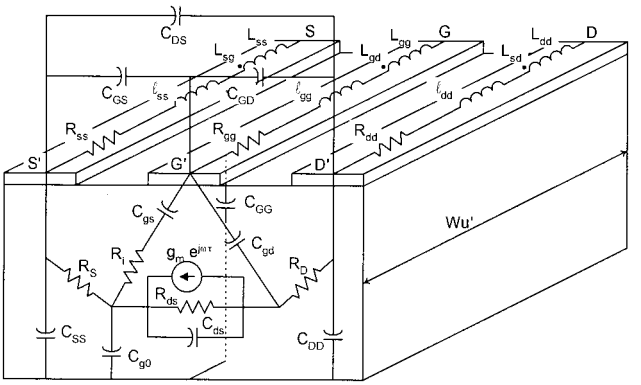

Figure 2 A section (slice) of the distributed small-signal FET model

model [12] is also determined by using the proposed method. Experimental results of the measured distributed noise sources of a PHEMT and its noise parameters up to 40 GHz are presented.

2. NOISE ANALYSIS

To model the distributed effects in FETs, a distributed model composed by N equal elemental sections (slices) is considered here [6, 10, 11]. The circuit elements, associated with an elemental section of width W'_u, are shown in Figure 2. It is assumed that the gate, drain, and source electrodes behave as transmission lines propagating waves through the section. The section width W'_u is defined as $W'_u = W_u/N$, where W_u is the gate width corresponding to a single gate finger. The FET total gate width is $W = W_u \cdot N_{bd}$, where N_{bd} is the number of gate fingers. Every elemental section is modeled as a noisy six-port (Fig. 2), whose ports are arranged as D-D'-G-G'-S-S', and this in turn is divided into two six-ports in cascade, whose cascade matrices are $\mathbf{A_1}$ and $\mathbf{A_2}$, respectively. The first one includes the electrode impedances and the second includes the intrinsic zone and the electrode capacitances C_{GG}, C_{DD}, C_{SS}, C_{GS}, C_{GD}, and C_{DS}.

The hybrid configuration ($e_{gs} - i_{ds}$) [13] is selected for the intrinsic FET noise sources, because its noise matrix $\mathbf{C}^{\text{int}}$ is basically frequency independent. Referring to Figure 2, the 6×6 noise-correlation matrix corresponding to six-port A_2 (including the thermal noise contribution of resistances R_S and R_D), expressed in cascade configuration as $\mathbf{C_{Ai}}$, is given by

$$\mathbf{C_{Ai}} = \mathbf{H} \cdot ((\mathbf{P_{HY}} \cdot \mathbf{C}^{\text{int}} \cdot \mathbf{P}^{\dagger}_{\mathbf{HY}}) + \mathbf{C}^{\mathbf{GD}}_{\mathbf{Y}}) \cdot \mathbf{H}^{\dagger} + (\mathbf{H_{YA}} \cdot \mathbf{Y_1}) \cdot \mathbf{C}^{\mathbf{R}}_{\mathbf{Z}} \cdot (\mathbf{H_{YA}} \cdot \mathbf{Y_1})^{\dagger}, \quad (1)$$

where the superscript † denotes the transpose-conjugate operator, $\mathbf{C}^{\text{int}}$ is the 2×2 intrinsic hybrid noise matrix of the following elemental section [9, 13]:

$$\mathbf{C}^{\text{int}} = \begin{bmatrix} C^{\text{int}}_{11} & C^{\text{int}}_{12} \\ C^{\text{int}}_{21} & C^{\text{int}}_{22} \end{bmatrix} = \begin{bmatrix} \overline{e^2_{gs}} & \overline{e_{gs} i^*_{ds}} \\ \overline{i_{ds} e^*_{gs}} & \overline{i^2_{ds}} \end{bmatrix}. \quad (2)$$

$\mathbf{C}^{\mathbf{GD}}_{\mathbf{Y}}$ is the 2×2 admittance-noise matrix of the gate-to-drain passive two-port, $\mathbf{P_{HY}}$ is the transformation matrix from the selected intrinsic noise-source configuration (in this paper, hybrid) to the admittance configuration, $\mathbf{H}$ is a transformation matrix used to convert the 2×2 intrinsic admittance-noise matrix of an elemental slice into a 6×6 cascade-noise matrix, $\mathbf{C}^{\mathbf{R}}_{\mathbf{Z}}$ is the 3×3 impedance noise matrix of the source-to-drain passive port, $\mathbf{Y_1}$ is the intrinsic 3×3 zone admittance matrix (Fig. 2), and $\mathbf{H_{YA}}$ is the matrix used to transform the 3×3 admittance-noise matrix into a 6×6 cascade matrix. The derivation of Eq. (1), including detailed expressions of the above matrices, is given in the Appendix. Note that other intrinsic correlation-matrix configurations $\mathbf{C}^{\text{int}}$ can be easily used with minor modifications, for example, if the admittance intrinsic-correlation matrix with gate- and drain-current correlation-noise sources is used [5], $\mathbf{P_{HY}}$ is replaced with the identity matrix.

It is assumed that the noise generated by the electrodes (resistances R_{dd}, R_{gg}, and R_{ss}) is thermal. Therefore, their 6×6 cascade-noise-correlation matrix $\mathbf{C_{Ae}}$ is given by

$$\mathbf{C_{Ae}} = \begin{bmatrix} \mathbf{C_{AD}} & \mathbf{0} & \mathbf{0} \\ \mathbf{0} & \mathbf{C_{AG}} & \mathbf{0} \\ \mathbf{0} & \mathbf{0} & \mathbf{C_{AS}} \end{bmatrix}, \quad (3)$$

where $\mathbf{C_{AD}}$, $\mathbf{C_{AG}}$, and $\mathbf{C_{AS}}$ are 2×2 cascade-correlation matrices of the drain, gate and source electrodes, respectively, which are computed from parasitic electrodes, and $\mathbf{0}$ is the 2×2 null matrix.

The 6×6 cascade-noise-correlation matrix for N elemental sections, $\mathbf{C_A}$, is written in terms of $\mathbf{C_{Ai}}$ and $\mathbf{C_{Ae}}$ as in Eqs. (1) and (3) as follows:

$$\mathbf{C_A} = \sum_{k=1}^{N} \mathbf{A}^{k-1} \cdot (\mathbf{C_{Ae}} + \mathbf{A_1} \cdot \mathbf{C_{Ai}} \cdot (\mathbf{A_1})^{\dagger}) \cdot (\mathbf{A}^{k-1})^{\dagger}, \quad (4)$$

where $\mathbf{A} = \mathbf{A_1} \cdot \mathbf{A_2}$.

To derive the total 2×2 cascade-noise-correlation matrix $\mathbf{C_{AT}}$ of the entire FET, two particular input-output port configurations (G-D' or G-D in Fig. 2) for N sections in cascade are considered, while the source port is connected to ground and the other ports (except the input and output ports) are open-circuited. Then, the nodal method is applied (using the concept of partition matrix [14] to split the ports into "external" and "internal" ones), and the effect of transistor pads (Fig. 3) is included. After straightforward algebraic derivations, the following expression for $\mathbf{C_{AT}}$ in terms of $\mathbf{C}^{\text{int}}$ is obtained:

$$\mathbf{C_{AT}} = \mathbf{C}_{\text{ext}} + \sum_{k=1}^{N} \mathbf{M}_k \cdot \mathbf{C}^{\mathbf{GD}}_{\mathbf{Y}} \cdot (\mathbf{M}_k)^{\dagger} + \sum_{k=1}^{N} \mathbf{M}_k \cdot \mathbf{P_{HY}} \cdot \mathbf{C}^{\text{int}} \cdot (\mathbf{M}_k \cdot \mathbf{P_{HY}})^{\dagger}, \quad (5)$$

where $\mathbf{C}^{\mathbf{GD}}_{\mathbf{Y}}$ and $\mathbf{P_{HY}}$ are defined as in the previous paragraphs (see also Appendix); $\mathbf{C}_{\text{ext}}$ is the correlation matrix corresponding to the thermal contributions of the access resistances, electrodes, and

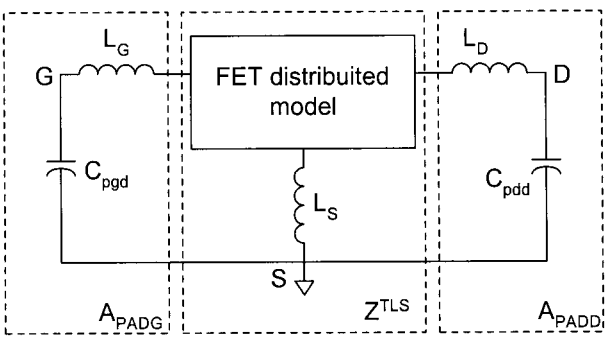

Figure 3 Distributed-noise model including external PADs

pads; $\mathbf{M}_k$ is the transformation matrix for slice n; and the last summation term in Eq. (5) is the intrinsic-noise-source contribution from all the individual slices ($\mathbf{C}_{\text{int}}$) to the total noise. Like $\mathbf{C}_{\mathbf{Y}}^{\mathbf{GD}}$ and $\mathbf{P}_{\mathbf{HY}}$, matrices $\mathbf{C}_{\text{ext}}$ and $\mathbf{M}_k$ are functions of the FET-equivalent circuit elements (computed from its S parameters) and room temperature only. From the FET total-noise correlation matrix given in Eq. (5), the FET noise parameters are readily computed using well-known formulas [15].

3. DETERMINATION OF THE INTRINSIC NOISE MATRIX FROM NOISE-FIGURE MEASUREMENTS

The transistor noise figure, measured at N_f frequency points, is a function of the source impedance Z_s^i ($i = 1 \ldots N_f$), and can be expressed in terms of its cascade-noise matrix $\mathbf{C}_{\mathbf{AT}}$, given by Eq. (5), as follows [15]:

$$F_{TRT}(Z_S^i) = 1 + \frac{\mathbf{Z} \cdot \mathbf{C}_{\mathbf{AT}} \cdot \mathbf{Z}^{\dagger}}{4kT_0 \text{Re}(Z_S^i)}; \quad \mathbf{Z} = [1 \quad (Z_S^i)^*], \tag{6}$$

where $T_0 = 290°$ K, k is the Boltzmann's constant, and $Z_S^i = R_S^i + j \cdot X_S^i$ is the source impedance corresponding to the i^{th} frequency. An arbitrary source can be used but, generally, a matched source is used to avoid oscillations. Substituting (5) into (6), the following linear equation system, for the i^{th} frequency point, is obtained for the unknowns C_{11}^{int}, C_{22}^{int}, $\text{Re}(C_{12}^{\text{int}})$, and $\text{Im}(C_{12}^{\text{int}})$ of the hybrid-noise correlation $\mathbf{C}^{\text{int}}$ corresponding to an elemental section [16]:

$$\Delta^i = \sum_{k=1}^{N} [J_1 \quad J_2 \quad J_3 \quad J_4]_k^i \cdot [C_{11}^{\text{int}} \quad C_{22}^{\text{int}} \quad \text{Re}\{C_{12}^{\text{int}}\} \quad \text{Im}\{C_{12}^{\text{int}}\}]^T; \quad (i = 1, \ldots, N_f), \tag{7}$$

$$(J_1)_k^i = |F_{11}^k|^2 + |Z_S^i|^2 |F_{21}^k|^2 + 2R_S^i \text{Re}(F_{11}^k F_{21}^{k*}) - 2X_S^i \text{Im}(F_{11}^k F_{21}^{k*}), \tag{8}$$

$$(J_2)_k^i = |F_{12}^k|^2 + |Z_S^i|^2 |F_{22}^k|^2 + 2R_S^i \text{Re}(F_{12}^k F_{22}^{k*}) - 2X_S^i \text{Im}(F_{12}^k F_{22}^{k*}), \tag{9}$$

$$(J_3)_k^i = 2\ \text{Re}(F_{11}^k F_{12}^{k*}) + 2|Z_S^i|^2 \text{Re}(F_{12}^k F_{22}^{k*}) + 2R_S^i \text{Re}(F_{12}^k F_{21}^{k*} + F_{11}^k F_{22}^{k*}), \tag{10}$$

$$(J_4)_k^i = -2\ \text{Im}(F_{11}^k F_{12}^{k*}) - 2|Z_S^i|^2 \text{Im}(F_{21}^k F_{22}^{k*}) - 2R_S^i \text{Re}(F_{11}^k F_{21}^{k*} - F_{12}^k F_{22}^{k*}), \tag{11}$$

where the superscript T indicates the transpose operator, and the elements F_{ij}^k of matrix $\mathbf{F}_k = \mathbf{M}_k \cdot \mathbf{P}_{\mathbf{HY}}$ [see Eq. (5)] depend only on the FET S parameters. The left side of Eq. (7) is a column matrix whose elements depend on the measured noise figure $F(Z_S^i)$ at every frequency point f_i and the following extrinsic-noise contribution:

$$\Delta^i = 4kT_0(F_{TRT}(Z_S^i) - 1) \cdot \text{Re}(Z_S^i) - \mathbf{Z} \cdot \left(\mathbf{C}_{\text{ext}} + \sum_{k=1}^{N} \mathbf{M}_k \cdot \mathbf{C}_{\mathbf{Y}}^{\mathbf{GD}} \cdot \mathbf{M}_k^{\dagger} \right) \cdot \mathbf{Z}^{\dagger}, \tag{12}$$

where it is assumed that the source impedance Z_S^i is known from the measurements. Generally, because a matched (Z_S^i not far away from 50Ω) noise source is used, F_{TRT} is also denoted by F_{50}. Note that expression (7) is an over-determined linear-equation system if a redundant number of frequency points ($N_f > 4$) are considered. Assuming a smooth frequency dependence for the unknowns C_{11}^{int}, C_{22}^{int}, $\text{Re}(C_{12}^{\text{int}})$, and $\text{Im}(C_{12}^{\text{int}})$ of Eq. (7), they are interpolated using an L-order polynomial, given by

$$C_{ij}^{\text{int}} = \sum_{l=0}^{L} f^l C_{ij}^l,$$

$$C_{ij}^{\text{int}} = C_{11}^{\text{int}},\ C_{22}^{\text{int}},\ \text{Re}\{C_{12}^{\text{int}}\} \text{ and } \text{Im}\{C_{12}^{\text{int}}\}. \tag{13}$$

In this work, a lineal approximation is considered ($L = 1$), and Eq. (7) is solved by least squares using pseudo-inverse calculation. The computed coefficients are used as initial values in an optimization algorithm that estimates C_{ij}^0 and C_{ij}^1 for the best fit of the computed F_{50}, from expression (7)–(11) to the measured noise figure in expression (12), using a robust Huber error function to discard "outliers." It is found that coefficients C_{22}^0 and C_{22}^1 produce the highest sensitivity in the transistor-noise parameters. According to decreasing sensitivity, the following order for the optimization parameters has been found: $\text{Re}(C_{12}^0)$, C_{11}^0, C_{22}^0, C_{22}^1, $\text{Re}(C_{12}^0)$, $\text{Im}(C_{12}^0)$, $\text{Re}(C_{12}^1)$, C_{11}^1.

Particular Case: Application to a "Noise Temperature" Simplified Model. As an application of the method proposed to extract a distributed noise model from noise-figure measurements, a simplified model for the intrinsic-noise correlation $\mathbf{C}^{\text{int}}$ is considered as a particular case. The noise-temperature model [7, 12] is a simplified (uncorrelated) model for an elemental section, where the following assumptions are made: the noise-source gate temperature is close to the room temperature T_a (then $C_{11}^{\text{int}} \approx 4 \cdot k \cdot T_a \cdot R_i$), and no correlation is assumed between the noise sources ($C_{12}^{\text{int}} = C_{21}^{\text{int}} = 0$). Then, at every frequency point there is only one nearly frequency-independent parameter, C_{22}^{int}, that can be obtained from the drain temperature T_d using Eq. (7):

$$C_{22}^{\text{int}^i} = 4k \frac{T_d}{R_{ds}} = \frac{\Delta^i - 4kT_a R_i \sum_{k=1}^{N} J_{1k}^i}{\sum_{k=1}^{N} J_{2k}^i}. \tag{14}$$

Note that the subscript i in R_i is different from the superscript i, which indicates the frequency index.

4. EXPERIMENTAL RESULTS

The elemental intrinsic-noise sources of a distributed-noise model of a 0.2-μm gate length, 4 × 15-μm gate-width PHEMT, biased with $V_{DS} = 1.5$ V and $I_{DS} = 17.4$ mA, were determined using the proposed method (described in section 3). The transistor intrinsic elements C_{gs}, C_{gd}, C_{ds}, R_i, R_{ds}, g_m, and τ, which are needed to compute the matrices required in Eqs. (7)–(12), are determined by applying scaling rules to a lumped-element model with the same topology as the intrinsic zone of an elemental section (see Fig. 2). For C_{gs}, C_{gd}, and C_{ds}, the electrode effects are also included and C_{g0} is a small parasitic channel to the substrate capacitance that can generally be neglected. Resistances R_S and R_D (Fig. 2), PAD capacitances C_{pgd} and C_{pdd}, and inductances L_G, L_D, and L_S (Fig. 3) are also computed by applying scaling rules to a lumped-element model and taking into account the electrode effects. Electrode capacitances C_{DD}, C_{GG}, C_{SS}, C_{DS}, C_{GD}, and C_{GS}, resistances R_{dd}, R_{gg}, and R_{ss}, and inductances L_{dd}, L_{gg}, L_{ss}, L_{sd}, L_{gd}, L_{sg}, ℓ_{dd}, ℓ_{gg}, and ℓ_{ss}, (Fig. 2) are calculated from odd- and even-mode decomposition using the analytical method proposed in [17].

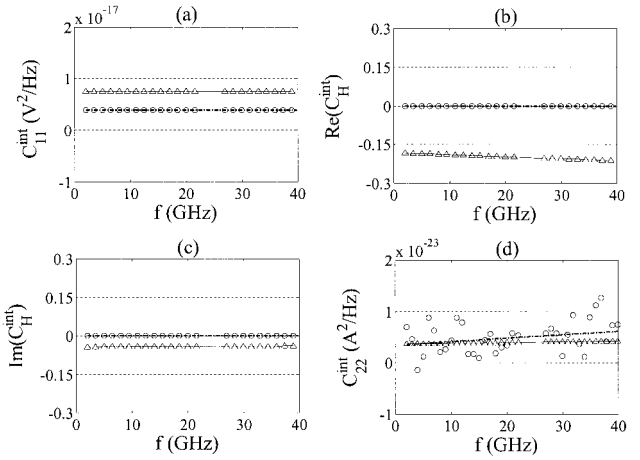

Figure 4 Extracted intrinsic-correlation matrix for a distributed model of a PHEMT elemental section using the proposed method, based on redundant noise-figure measurements and lineal polynomial frequency behavior approximation [Eqs. (7)–(13)] (-△-), applying the "noise temperature" model [Eq. (14)] (-○-), and interpolating the "noise temperature" model results (-·-)

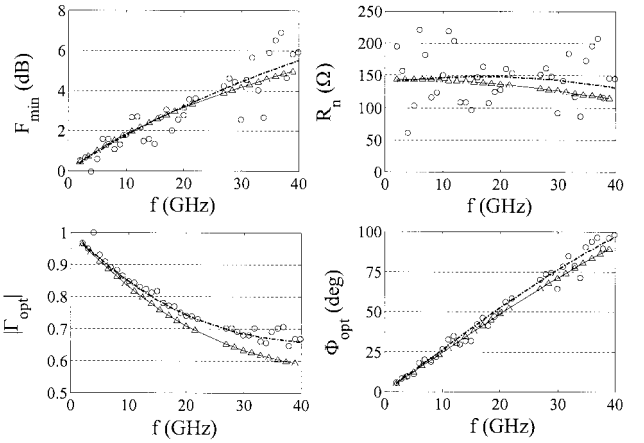

Figure 5 PHEMT noise parameters computed from Eq. (5), using the measured $\mathbf{C}^{\text{int}}$ (Fig. 4) computed using the proposed method, based on redundant noise-figure measurements and lineal polynomial frequency behavior (Eqs. (7)–(13)] (-△-), applying the "noise temperature" model [Eq. (14)] (-○-), and interpolating the noise-temperature-model results (-·-)

The transistor-noise figure was measured with the experimental setup described in [18]. Figure 4 plots the extracted intrinsic correlation matrix, given by Eq. (2), in hybrid configuration (with gate-voltage and drain-current sources) of an elemental section of the PHEMT using Eqs. (7)–(13). Results show that the hybrid-matrix elements are almost frequency independent and they can be interpolated using a linear polynomial. In Figures 4(b) and 4(c), the real and imaginary parts of the correlation factor C_H are plotted, respectively, where C_H is defined as $C_H = C_{12}^{\text{int}}/\sqrt{C_{11}^{\text{int}} \cdot C_{22}^{\text{int}}}$. It can be seen that C_H is different from zero and basically real. In Figure 4(d), the results of C_{22}^{int} are also compared to the "noise temperature" model, computed from Eq. (14) at every frequency point. Some dispersion of the "noise temperature" model results is observed, due to measurement uncertainties, which are directly translated to C_{22}^{int}. However, the average value from direct extraction of C_{22}^{int} is close to the hybrid model. Likewise, C_{11}^{int} computed from the "noise temperature" model (in which the gate temperature is assumed to be the room temperature) differs from the hybrid model, as seen in Figure 4(a). In fact, the value of the hybrid model is larger than that of the "noise temperature" model, which implies that the gate temperature is bigger than the room temperature.

In Figure 5, the PHEMT noise parameters, computed from (5), using the measured $\mathbf{C}^{\text{int}}$, are presented. It can be observed that results obtained from the optimized intrinsic noise matrix are close to the results obtained from the "noise temperature" model (Eq. (14)). The assumption of $C_H = 0$ mainly affects $|\Gamma_{\text{opt}}|$, in agreement with the literature [13], and the differences in R_n and $F_{\min}$ are mainly due to the differences in C_{11}^{int}, C_{22}^{int}, and, to a lesser extent, to C_{12}^{int}. Therefore, the method here proposed reduces measurement error effects in the determination of noise parameters using both, uncorrelated and correlated distributed noise models.

In Figure 6, the PHEMT noise parameters extracted from the F_{50} method applied to the distributed model are compared to those obtained by applying the F_{50} method to a lumped model [9]. In both cases, the hybrid intrinsic model is considered. The results show a similar frequency response; however, some differences are noticed. When the distributed model is applied, the PHEMT minimum-noise figure is somewhat higher and its frequency response presents a sharper curvature than that of the lumped model. Likewise, R_n is somewhat higher and $|\Gamma_{\text{opt}}|$ somewhat smaller for the distributed model than for the lumped model, while Φ_{opt} remains nearly invariable. These results are mainly due to the thermal effects of the electrodes, according to previous works in the literature [10, 19], and, to a lesser extent, due to the differences between the topologies assumed in each model.

5. CONCLUSION

A method for the determination of a distributed FET noise model based on noise figure F_{50} measurements only, without the necessity of a tuner to measure the four noise parameters, has been presented. Arbitrary intrinsic FET noise models (which include correlation) with smooth frequency dependence can be extracted. In this paper, the hybrid configuration for the intrinsic-noise matrix of an elemental section, $\mathbf{C}^{\text{int}}$, has been used. This method has been applied to a PHEMT. Experimental results up to 40 GHz show that the elements of $\mathbf{C}^{\text{int}}$ (hybrid) have a linear-frequency dependence and that the proposed method reduces the uncertainty in the determination of the intrinsic-noise sources. Application of the distributed model allows the extraction of the FET noise parameters, including the thermal-noise contribution due to the FET electrodes. The distributed effects are mainly observed in the

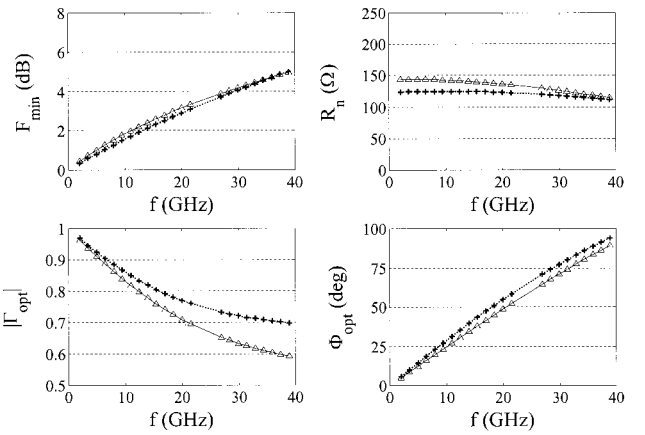

Figure 6 PHEMT noise parameters extracted using the proposed method with a distributed model (-△-) and a lumped model (-+-)

magnitude of the optimum reflection coefficient $|\Gamma_{opt}|$, in the minimum noise figure F_{min}, its frequency response (which tends to increase), and, to a lesser extent, in the equivalent resistance R_n, and in the phase of the optimum reflection coefficient ϕ_{opt}.

APPENDIX: NOISE CORRELATION MATRIX OF THE INTRINSIC ZONE OF AN ELEMENTAL SECTION

Figure 2 shows an elemental section of width W'_u, where the intrinsic-noise sources are modeled in a hybrid configuration for $(e_{gs} - i_{ds})$ [13]. First, the intrinsic correlation matrix $\mathbf{C}^{int}$ is transformed into an admittance configuration using a transformation matrix $\mathbf{P_{HY}}$, and the noise contribution $\mathbf{C_Y^{GD}}$ of the capacitance C_{gd} is added as follows:

$$\mathbf{C_Y^{int}} = \mathbf{P_{HY}} \cdot \mathbf{C^{int}} \cdot \mathbf{P_{HY}^{\dagger}} + \mathbf{C_Y^{GD}}, \tag{A1}$$

$$\mathbf{P_{HY}} = \begin{bmatrix} Y_{11}^{int\_GD} & 0 \\ Y_{21}^{int\_GD} & 1 \end{bmatrix}; \quad \mathbf{Y^{int\_GD}} = \mathbf{Y^{int}} - \mathbf{Y^{GD}}; \tag{A2}$$

$$\mathbf{Y^{GD}} = j\omega \begin{bmatrix} C_{gd} & -C_{gd} \\ -C_{gd} & C_{gd} \end{bmatrix}; \quad \mathbf{C_Y^{GD}} = 2kT_a(\mathbf{Y^{GD}} + \mathbf{Y^{GD\dagger}}), \tag{A3}$$

where $\mathbf{Y^{int}}$ is the two-port (2×2) admittance matrix of the active part without including R_S and R_D, and T_a is room temperature. Next, the two-port configuration (G'-D', with S' connected to ground) is transformed into a three-port (D'-G'-S') configuration by applying a transformation matrix, $\mathbf{H_1}$, and the noise contribution $\mathbf{C_Z^R}$ of the resistances R_S and R_D is added; thus, we obtain

$$\mathbf{C_{Zb}} = (\mathbf{Y_{3\times3}^{INT}})^{-1} \cdot (\mathbf{H_1} \cdot \mathbf{C_Y^{int}} \cdot \mathbf{H_1^{\dagger}}) \cdot ((\mathbf{Y_{3\times3}^{INT}})^{-1})^{\dagger} + \mathbf{C_Z^R}, \tag{A4}$$

$$\mathbf{H_1} = \begin{bmatrix} 1 & 0 \\ 0 & 1 \\ -1 & -1 \end{bmatrix}; \quad \mathbf{Y_{3\times3}^{INT}} = \mathbf{H_1} \cdot \mathbf{Y^{int}} \cdot \mathbf{H_1^{\dagger}} + \begin{bmatrix} 0 & 0 & 0 \\ 0 & 0 & 0 \\ 0 & 0 & j\omega C_{g0} \end{bmatrix};$$

$$\mathbf{C_Z^R} = 4kT_a \begin{bmatrix} 0 & 0 & 0 \\ 0 & R_D & 0 \\ 0 & 0 & R_S \end{bmatrix}, \tag{A5}$$

where $\mathbf{Y_{3\times3}^{INT}}$ is a transformation matrix from admittance configuration to impedance configuration [15]. Then, a transformation from impedance configuration to admittance configuration is made using $\mathbf{Y_1}$, and the three-port (G'-D'-S') configuration is transformed into a six-port (D-D'-G-G'-S-S') configuration by applying a transformation matrix, $\mathbf{H_{YA}}$ as follows:

$$\mathbf{C_{Ai}} = (\mathbf{H_{YA}} \cdot \mathbf{Y_1}) \cdot \mathbf{C_{Zb}} \cdot (\mathbf{H_{YA}} \cdot \mathbf{Y_1})^{\dagger}, \tag{A6}$$

$$\mathbf{Y_1} = \left((\mathbf{Y_{3\times3}^{INT}})^{-1} + \begin{bmatrix} 0 & 0 & 0 \\ 0 & R_D & 0 \\ 0 & 0 & R_S \end{bmatrix} \right)^{-1};$$

$$\mathbf{H_{YA}} = \begin{bmatrix} 0 & 0 & 0 & -1 & 0 & 0 \\ 0 & -1 & 0 & 0 & 0 & 0 \\ 0 & 0 & 0 & 0 & 0 & -1 \end{bmatrix}^{\dagger}, \tag{A7}$$

where $\mathbf{Y_1}$ is the admittance matrix of the intrinsic zone (Fig. 2). Substituting (A1) and (A4) into (A6), the expression of the cascade-correlation matrix for the active part of the elemental section is found [see Eq. (1)], where the transformation matrix $\mathbf{H}$ is given by

$$\mathbf{H} = \mathbf{H_{YA}} \cdot \mathbf{Y_1} \cdot (\mathbf{Y_{3\times3}^{INT}})^{-1} \cdot \mathbf{H_1}. \tag{A8}$$

ACKNOWLEDGMENTS

This work has been supported by Spanish Government grants TIC2000-0144P4-02 and ESP2002-04141-C03-02 (MCYT), and a scholarship from CONACYT–Mexico.

REFERENCES

1. W. Heinrich and H. Hartnagel, Wave propagation on MESFET electrodes and its influence on transistor gain, IEEE Trans Microwave Theory Tech 35 (1987), 1–8.
2. A. Cidronali, G. Collodi, A. Santarelli, G. Vinnini, and G. Manes, Millimeter-wave FET modeling using on-wafer measurements and EM simulation, IEEE Trans Microwave Theory Tech 50 (2002), 425–432.
3. L. Sunyoung, P. Roblin, and O. Lopez, Modeling of distributed parasitics in power FETs, IEEE Trans Electron Devices 49 (2002), 1799–1806.
4. W. Heinrich, Distributed analysis of submicron-MESFET noise properties, IEEE MTT-S Dig (1988), 327–330.
5. A. Cappy, A. Vanovershelde, M. Schortegen, C. Versaeyen, and G. Salmer, Noise modeling in submicrometer-gate two-dimensional electron-gas field-effect-transistor, IEEE Trans Electron Devices 32 (1985), 2787–2795.
6. A. Abdipour and A. Pacaud, Temperature noise constants extraction of mm-wave FET's from measured S- and noise parameters, IEEE MTT-S Dig (1996), 1723–1726.
7. M. Pospieszalski, Modeling of noise parameters of MESFET's and MODFET's and their frequency and temperature dependence, IEEE Trans Microwave Theory Tech 37 (1989), 1340–1350.
8. A. Lázaro, L. Pradell, and J.M. O'Callaghan, Method for measuring noise parameters of microwave two-port, Electron Lett 34 (1998), 1332–1333.
9. A. Lázaro, L. Pradell, and J.M. O'Callaghan, FET noise parameter determination using a novel technique based on 50Ω noise figure measurements, IEEE Trans Microwave Theory Tech 47 (1999), 315–324.
10. L. Escotte and J.-C. Mollier, Semidistributed model of millimeter-wave FET for *S*-parameter and noise-figure predictions, IEEE Trans Microwave Theory Tech 38 (1990), 748–753.
11. K.B. Niclas and B.A. Tucker, On noise in distributed amplifiers at microwave frequencies, IEEE Trans Microwave Theory Tech 3 (1983), 661–668.
12. P.J. Tasker, W. Reinert, B. Hughes, J. Braunstein, and M. Schlechtweg, Transistor noise parameter extraction using a 50 Ω measurement system, IEEE MTT-S Dig (1993), 1251–1254.
13. R.A. Pucel, W. Struble, R. Hallgren, and U.L. Rohde, A general noise de-embedding procedure for packaged two-port line active devices, IEEE Trans Microwave Theory Tech 40 (1992), 2013–2024.
14. V. Rizzoli and A. Lipparini, Computer-aided noise analysis of linear multiport networks of arbitrary topology, Trans Microwave Theory Tech 33 (1985), 1507–1512.
15. H. Hillbrand and P. Russer, An efficient method for computer aided noise analysis of linear amplifier networks, IEEE Trans Microwave Theory Tech 23 (1976), 235–238.
16. M.C. Maya, A. Lázaro, and L. Pradell, Determination of FET noise parameters from 50Ω noise-figure measurements using a distributed noise model, GaAs Conf, 2002, pp. 225–228.
17. R.L. Chang, Modelling and analysis of GaAs MESFETs considering the wave propagation effect, IEEE MTT-S Int Microwave Symp Dig (1989), 371–374.
18. A. Lazaro, M.C. Maya, and L. Pradell, Measurement of on-wafer transistor noise parameters without a tuner using a unrestricted noise sources, Microwave J 45 (2002), 20–46.
19. A. Abdipour and A. Pacaud, A new semidistributed model for the noise and scattering parameters of the M(H)MIC FETs, IEEE SBMO/IEEE MTT-S IMOC'95 Proc, 1995, pp. 755–760.